DOI: 10.1021/ma901952p

Macromolecules
ARTICLE

Interfacial Interactions in PP/MMT/SEBS Nanocomposites

Zulima Martín,*,† Ignacio Jiménez,‡ M. Ángeles Gómez,† Harald Ade,§ and David A. Kilcoyne⊥

†*Instituto de Ciencia y Tecnología de Polímeros, ICTP-CSIC. Juan de la Cierva 3, 28006 Madrid, Spain,*
‡*Instituto de Ciencia de Materiales de Madrid, ICMM.-CSIC. Campus de Cantoblanco, 28049 Madrid, Spain,*
§*Department of Physics, North Carolina State University, Raleigh, North Carolina 27695, and*
⊥*Advanced Light Source, Lawrence Berkeley National Laboratory, Berkeley, California 94720*

Received September 2, 2009; Revised Manuscript Received November 18, 2009

ABSTRACT: The intercalation capability of poly(styrene-*b*-ethylene butylene-*b*-styrene) (SEBS) in nanocomposites of isotactic polypropylene (PP) with 5 wt % of organically modified montmorillonite (C20A), prepared by melt blending, has been investigated. X-ray diffraction (XRD) and transmission electron microscopy (TEM) studies have shown the presence of intercalated structures in the nanocomposite. In a previous research, we studied the intercalation capability of a commercial compatibilizer.[1] Those results, with the study we present in this work, allow us a better understanding of the mechanism of compatibilization and a deeper characterization of the structure and morphology of the nanocomposite. Scanning transmission X-ray microscopy (STXM) has been used. Because of the excellent chemical sensitivity and the high spatial resolution (∼40 nm) of this technique, we have proved that C20A is not in direct contact with the PP phase because the clay is always located inside the elastomer domains. The elastomer is surrounding the nanoclay, hindering the clay exfoliation and preventing its dispersion in the PP matrix. On the other hand, we have observed that the presence of the clay caused the SEBS particles to become elongated in shape and retarded the coalescence of the elastomer particles.

Introduction

Phenomena and processes at the nanometric scale have opened revolutionary possibilities in the development of new nanostructured materials. In polymer systems, the addition of layered silicates leads to a great improvement in the properties of the matrix such as thermal stability and mechanical performance with very low filler contents. This is because the high surface area of these particles with nanometric dimensions increases the interfacial interactions between matrix and clay.[2−5] Therefore, the key factor for the enhancement in performance of the polymer/clay nanocomposites is the dispersion of the filler in the matrix since the final properties depend on the structure and morphology generated during the processing. Consequently, a significant research effort is dedicated to characterize the nanostructure in polymer nanocomposites.

In this study, we have prepared isotactic polypropylene/montmorillonite/poly(styrene-*b*-ethylene butylene-*b*-styrene) elastomer composites from the melt considering that this processing method is the most attractive for industrial application.[6−10] The addition of SEBS as a third component in the composite is intended to provide a better dispersion and intercalation of the silicate and also to provide a toughness improvement. Montmorillonite is the most commonly used layered silicate for the preparation of nanocomposites because of its high aspect ratio, large surface area, and surface reactivity. Its structure consists on the stacking of aluminosilicate layers ∼1 nm thick, with a regular spacing between them of ∼1.5 nm. Its high cation exchange capacity offers a way of modifying the interlayer spacing to make it larger and more compatible with polymers. However, unlike polymers with polar groups like polyamides,[3,6,11−13] in nonpolar polymers like polypropylene (PP) the organic modification of the clay is not enough to achieve a good level of dispersion and hardly leads to mixed structures.[14−19] Therefore, compatibilizers like polypropylene-*graft*-maleic anhydride (PP-*g*-MA) are commonly used to improve interactions between the organic polymer and the inorganic filler.[20−23]

In this work, we have studied the intercalation capability of a styrene−ethylene butylene−styrene triblock copolymer, SEBS, as an alternative to the use of common compatibilizers, such as the PP-*g*-MA mentioned above, in PP/montmorillonite nanocomposites. In PP nanocomposites, an elastomer phase is normally used to compensate for the reduction of toughness caused by adding inorganic fillers.[24,25] In principle, SEBS can aid the polypropylene chains to get into the nanoclay layers. Therefore, it can be expected that SEBS favors the intercalation and/or exfoliation. On the other hand, it has been reported that in these kinds of blends of immiscible polymers, e.g., PS/PP[26] or PBT/PE,[27] the nanoclay acts modifying the interphase properties and so improving the compatibility between the different polymeric phases. SEBS presents a phase-separated morphology, and consequently, its interactions with the montmorillonite and its intercalation capability will be very different from the ones of common compatibilizers. The aim of this work is to investigate the structure, morphology, and interfaces of isotactic polypropylene−clay−elastomer nanocomposites prepared by melt mixing. X-ray diffraction (XRD) and transmission electron microscopy (TEM) are used to characterize the intercalation capability of the polymers. TEM microscopy alone cannot provide conclusive information about the compatibilization role of SEBS in the PP−clay system, since although the lack of chemical contrast between the SEBS and PP polymeric phases could be overcome by OsO_4 staining, the different TEM magnifications needed to observe the rubber phase (in the range of micrometers) and the clays (in the range of nanometers) would make difficult to observe the three components simultaneously. Besides, no compositional chemical information is provided by this technique.

*Corresponding author. E-mail: amiluz@hotmail.com.

 Published on Web 12/08/2009

The nanocomposite morphology was also investigated by scanning transmission X-ray microscopy (STXM), which has proved to be a very powerful tool for the characterization of structured soft condensed matter nanomaterials.[28−30] A complete characterization requires both a microscopy technique with high spatial resolution (submicrometric) and a spectroscopy technique with high chemical sensitivity. STXM, based on the different X-ray absorption of each component, can perform chemical mapping at nanometric scale of thin film composites, and hence both visual and compositional chemical information are provided at the same time.[31] STXM has allowed us to observe simultaneously the three components in the nanocomposites investigated supplying excellent information on the interactions among polymers and nanoclay and the exact localization of the organoclay with respect to the two polymers.

Experimental Section

Materials. The polypropylene (PP) used as matrix was an isotactic homopolymer, with a polydispersity of 4.77, provided by REPSOL. It is characterized by an isotacticity of 95%, determined by solution NMR, and a viscosity average molecular weight of 179 000 g/mol, obtained by intrinsic viscosity measurements.[1,32] The organically modified montmorillonite (MMT) clay used in this study was Cloisite 20A (C20A) obtained from Southern Clay Products.[1] The individual platelets are typically 1 nm in thickness, with an aspect ratio larger than 50. The interlayer spacing, determined by XRD, is d_{001} = 2.52 nm. The elastomer used was a triblock copolymer SEBS (Calprene H-6110) provided by DYNASOL, with 30 wt % of styrene content, a molecular weight value of M_w = 85 000 g/mol, and M_w/M_n = 1.45, as determined by gel permeation chromatography (GPC).

Preparation of PP−MMT Composites. Polymer blends and composites were prepared by melt blending in a Haake Rheomix 600 internal mixer attached to a Haake Rheocord 90 corotating twin-screw mixing chamber. A temperature of 190 °C, mixing time of 5 min, and a rotor speed of 100 rpm were determined to be the optimum processing conditions. In the composite, PP/C20A/SEBS (80/5/15), clay loading was 5 wt % as it is demonstrated to be the optimum content for mechanical performance.[16,18,19,33,34] In order to compare the compatibilizer activity of SEBS with commercial compatibilizers, the elastomer content was 15 wt % because as seen in the literature weight ratios of clay/commercial compatibilizers of 1/3 give better results of clay dispersion.[1,19,20] Binary composites PP/C20A (95/5) and binary PP/SEBS blends (90/10) and (80/20), with 10 and 20 wt % elastomer content, respectively, were used for comparison. Films of the nanocomposite material were compression-molded at 100 Mbar by heating the pellets at 190 °C for 5 min with subsequent quenching of the formed film between water-cooled metal plates.

Characterization. *XRD*. X-ray diffraction (XRD) was used to measure the interlayer spacing of the clay. XRD patterns were obtained at room temperature using a Philips PW 1050/70 diffractometer, at 1°/min in a 2θ range between 2° and 35° using Ni-filtered Cu Kα radiation.

TEM. The dispersion of the nanoclays and composite morphology on a microscopic scale were examined by transmission electron microscopy (TEM). Images were obtained with a Philips Tecnai 20 microscope. Ultrathin sections, 50−100 nm in thickness, were cryogenically microtomed with a diamond knife at ∼−60 °C. Sections were collected on copper TEM grids.

STXM. To identify the chemical composition of the composites and to observe simultaneously all the components in the nanostructure, scanning transmission X-ray microscopy (STXM) measurements were conducted using the STXM at BL5.3.2 of the Advanced Light Source at Lawrence Berkeley National Laboratory.[35,36] STXM allows a detailed chemical and compositional analysis with excellent chemical sensitivity and a high spatial resolution. The BL 5.3.2 STXM can provide images with ∼30 nm spatial resolution for X-ray photons of 250−600 eV, with an energy resolution of about 0.1 eV. The energy range includes the most important absorption edges in polymer chemistry: C(1s) at 280 eV, N(1s) at 400 eV, and O(1s) at 520 eV. We have used NEXAFS microscopy to obtain images with nanometric resolution and absorption contrast between the two polymer components, making use of the different X-ray absorption of the different components. The spectra shown are normalized to the maximum height for comparison purposes. Image sequences, used to provide detailed chemical mapping, were converted to chemical component maps using pixel-by-pixel curve fitting with suitable XANES spectra from reference components. Details about this instrument and experiment can be found elsewhere.[36] To obtain the map shown below, a complete sequence of images at photon energies encompassing the C(1s) region was recorded corresponding to a typical XANES energy scan. In this way, each pixel, representing a morphological and spatial dimension, contains a full XANES spectrum.[1]

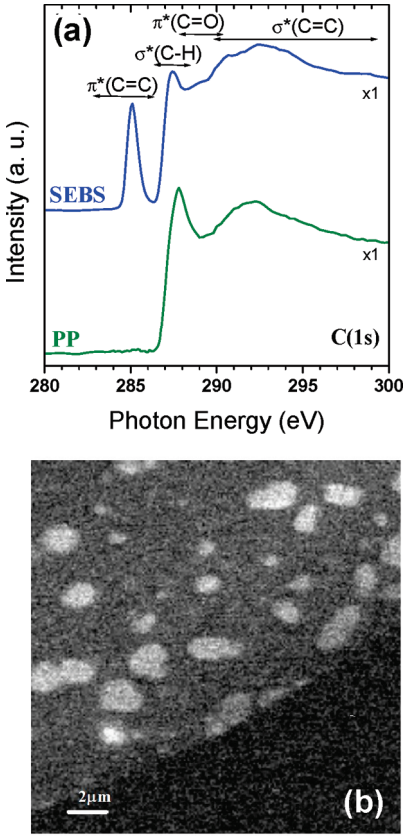

Figure 1. (a) NEXAFS spectra at the C(1s) edge of pristine components: PP and SEBS. (b) STXM image at 285 eV of an area at the edge of a section of PP/SEBS (80/20) (20 μm × 20 μm), displayed in optical density. Lighter regions indicate stronger X-ray absorption.

Results and Discussion

PP/SEBS. Prior to the analysis of the composite PP/C20A/SEBS, we have studied the binary blends PP/SEBS to identify the size and shape of the elastomer domains before adding the nanoclay. This let us know how they are affected by the presence of the C20A montmorillonite in the composite. We have investigated PP/SEBS blends in compositions (90/10) and (80/20).

Figure 1a shows XANES spectra measured at the C(1s) edge from the reference components used in the blend, PP and SEBS. The spectra are shown normalized to the maximum height for comparison purposes. At 285 eV, the

Table 1. Surface Energy of Polymer Components in PP/C20A/SEBS

polymer	surface energy (mN/m)	dispersive part (mN/m)	polar part (mN/m)
PP	30.1	30.1	0
PE	35.7	35.7	0
PB	33.6	33.6	0
PS	40.7	34.5	6.1

C-1s → $\pi^*_{C=C}$ region, SEBS shows a peak due to the absorption of the styrene group. The characteristic peak of polyolefins at 288 eV is in the C-1s → σ^*_{C-H} region, at the onset of the σ^* states.[37] Figure 1b shows an STXM image of PP/SEBS (80/20) acquired at 285 eV in absorption mode, i.e., with the bright areas corresponding to the maximum absorption occurring at the styrene groups of SEBS domains. We can observe simultaneously the two immiscible polymeric phases, with the bright SEBS domains as round droplets uniformly distributed in the dark PP continuous phase. A statistical analysis of particle shape and size, made from 100 particles of different slices of each sample, indicates an average aspect ratio (AR) close to 1 and an average diameter near 1 μm. For the composition (90/10) the AR is 1.05 ± 0.15, and for composition (80/20) is 1.30 ± 0.50. Furthermore, we observed a slight increase of the domain size with rubbery content, from 0.8 μm for blend (90/10) to 1 μm for the blend (80/20). The increase in aspect ratio and size can be explained by the coalescence of SEBS domains when the elastomer content increases.

The STXM results are in qualitative agreement with a previous SEM study[38] of these blends, where the droplet dispersion morphology was observed. In that study the rubbery phase was extracted with heptane to observe the morphology of the cavities that corresponded to the volume initially occupied by the rubbery phase; thus, the SEBS domains were not directly measured. The cavities measured by SEM in the heptane-extracted blend (80/20) appears with an average diameter of ~2.5 μm, i.e., larger than in the direct measurements by STXM, although maintaining the aspect ratio of ~1.3. With STXM the SEBS domains are directly observed without any artifact from the use of solvants.

PP/C20A/SEBS. We have studied the structure and morphology of the 80/5/15 PP/C20A/SEBS composite. Although we observed that the rubbery phase does not mix with PP matrix in binary blends, we do not know in principle how the presence of the nanoclay could affect to SEBS dispersion. On the one hand, it has been seen that organically modified layered silicates can work as a compatibilizer for immiscible polymer blends.[26,27,39] On the other hand, SEBS has certain polarity between the main chain and the styrene group that reveals as a polar component in the surface energy (Table 1[40]). This fact in addition to its flexibility explains that SEBS chains can get into the interlayer spacing of the nanoclay, facilitating also the intercalation of PP chains. First, we used XRD to evaluate the intercalation capability of the polymers. Figure 2a shows XRD patterns of pristine components (PP, C20A, and SEBS) and XRD patterns of the composites, PP/C20A(95/5) and PP/C20A/SEBS (80/5/15). It is clearly seen (Figure 2a) that neither the presence of C20A or SEBS nor preparation of composites method alters the monoclinic α structure of the isotactic PP (i-PP) since the composites maintain the same diffraction peaks as the reference i-PP.[41,42] The level of intercalation in C20A was evaluated on the basis of the change of the clay interlayer spacing from the 2θ position of the (001) diffraction peak (Figure 2b). Pristine clay has a d spacing (d_{001}) of 2.52 ± 0.05 nm. Whereas the presence of diffraction peaks in the composites indicates that the clay was not fully exfoliated, the increase in the d-spacing observed in both composite indicates the formation of intercalated structures.[4] In the nanocomposite without elastomer the interlayer spacing of the C20A increases slightly from 2.52 ± 0.05 to 2.59 ± 0.05 nm. In the composite with SEBS the interlayer distance increases up to 3.28 ± 0.05 nm, confirming the better intercalation capability in the presence of SEBS. The XRD peak position indicates that PP/C20A/SEBS has an intercalated structure, and the decrease in the intensity of the basal peak indicates the presence of disordered or exfoliated regions.[18,43] XRD does not allow a more detailed characterization of the structure of the nanocomposites. We know that the nanoclay is intercalated, but we do not know how C20A interacts with the polymers.

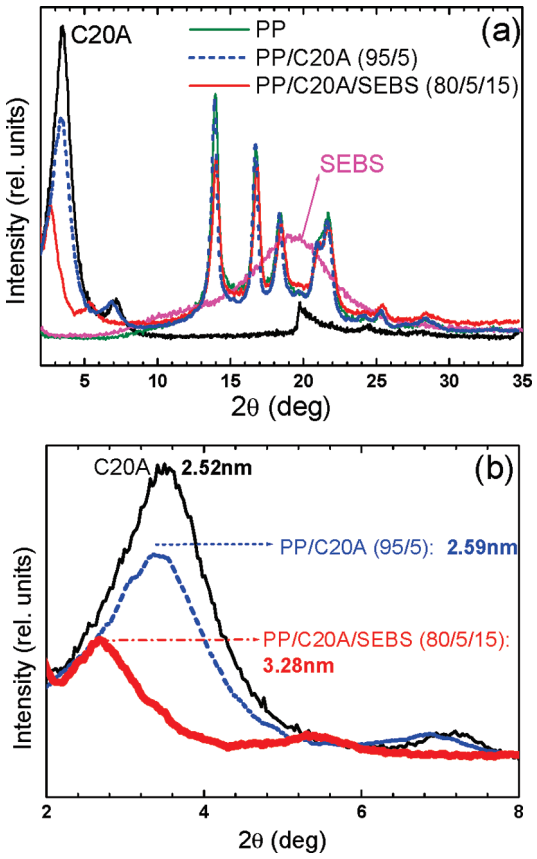

Figure 2. XRD patterns for pristine clay and for nancocomposites. Inset number denotes the d_{001} of clay.

A further characterization of the clay dispersion and morphology of the nanocomposites was observed by TEM (Figure 3). At the microscale (left column, 1 μm scale bar) in the binary nanocomposite, PP/C20A (95/5) (Figure 3a), we can observe that the nanoclay is not well dispersed. C20A appears in straight stacks spaced 1 μm approximately. Nevertheless, these stacks are smaller than in pristine montmorillonite, with typical dry particle size 2−13 μm.[44] In the nanocomposite with 15 wt % of SEBS (Figure 3c), the morphology observed is quite similar to the binary sample, but the stacks are not so well lined up and their aspect ratio are smaller. From the TEM images we cannot differentiate the PP and SEBS regions, and hence, we do not know which is the polymer component interacting with the C20A montmorillonite, a question that will be solved by STXM. To observe in more detail the opening of the layered structure of C20A, the right column of Figure 3 shows higher magnification images (50 nm scale bar). Figure 3b corresponds to the

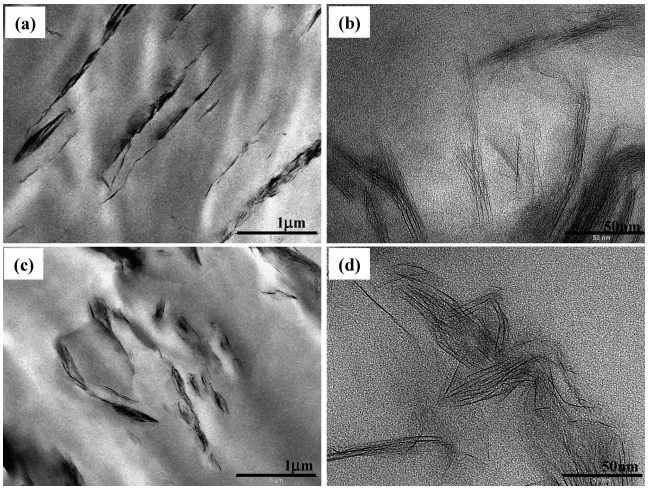

Figure 3. TEM images of the nanocomposites (PP/C20A (95/5), top row; PP/C20A/SEBS (80/5/15), bottom row) at different magnifications (low magnification: left column; high magnification: right column).

Table 2. Interlayer Distances of Nanocomposites

	interlayer distance (nm)	
SEBS (wt %)	from TEM	from XRD
0	2.4 ± 0.3	2.59 ± 0.05
15	3.0 ± 0.8	3.28 ± 0.05

binary nanocomposite and shows that the nanoclay appears mostly in stacks, although there are a few intercalated regions in parallel planes confirming a mixed morphology. The interlayer distances measured in various locations of several TEM images provide an average value that is in agreement with the XRD results (Table 2). In the nanocomposites with SEBS (Figure 3d), the morphology is very different. According to the XRD results (Table 2), the interlayer spacing observed is larger than in the binary composite. The structure presents a mixed morphology. Stacks coexist with intercalated regions and few individual exfoliated layers. Anyhow, the dispersion of the clay is far from being optimum. The structure is disordered; the clay platelets do not appear lined up, but bent and twisted. This type of twisted structure is different from that observed in other polymer/clay nanocomposites using commercial compatibilizers, where a better dispersion of the nanoclay is achieved and the delamination of the montmorillonite starting from the edge of the layer, like fanning out, is observed.[1,19] When SEBS is incorporated, the exfoliation mechanism is different and appears related to the droplet dispersion of the SEBS phase in the PP matrix.

To simultaneously observe and identify the three components of the PP/C20A/SEBS nanocomposite and discern which is the polymer component interacting with the clay, a detailed study was carried out using STXM.

Figure 4a shows the XANES normalized spectra measured at the C(1s) edge from the reference components, that is, from pristine PP, C20A, and SEBS. The most characteristic feature of the PP reference is the dominant peak at 288 eV corresponding to σ^*_{C-H} states and the absence of any feature related to double bonds. The SEBS reference is mainly identified by the $\pi^*_{C=C}$ peak of the styrene groups at 285 eV. The most characteristic features of the C20A signal are the presence of a broader $\pi^*_{C=C}$ peak at slightly lower energy compared to SEBS, corresponding to aliphatic

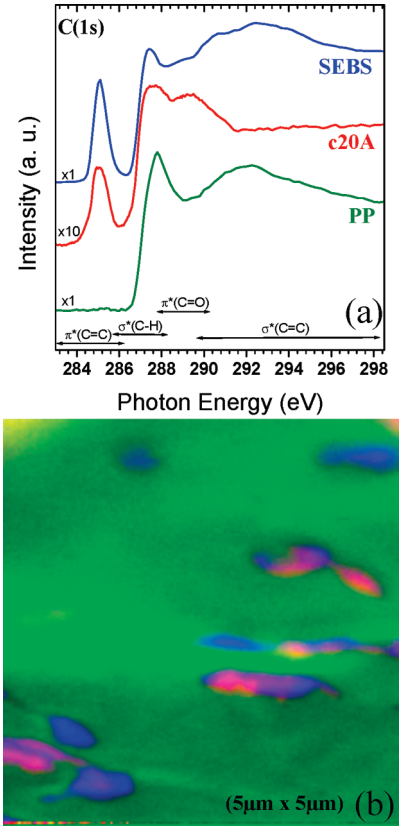

Figure 4. (a) NEXAFS spectra at the C(1s) edge of pristine components: PP (green), C20A (red), and SEBS (blue). (b) STXM composition map of PP/C20A/SEBS (80/5/15) recorded from 272 up to 320 eV (5 μm × 5 μm). The color intensities in STXM are relative to each component.

double bonds, and a broad peak at 289.5 eV in the σ^*_{C-C} region that is absent in the other two references. Figure 4b shows the PP/C20A/SEBS (80/5/15) chemical composition map derived from STXM measurements in the photon energy range from 272 to 320 eV. The different colors represent different component materials in the nanocomposite. Green regions correspond to the coincidence with the XANES spectrum of PP, blue ones to the spectrum of SEBS, and red ones correspond to C20A. Intermediate colors indicate the presence of several components in one pixel space. From Figure 4b there are three direct observations of importance, which will be discussed below in more detail: (i) it is clear that SEBS is the polymer component interacting directly with the C20A montmorillonite, (ii) the phase separation between SEBS and PP components remains, and (iii) the SEBS droplets are largely deformed in shape due to the presence of C20A.

Regarding the size and shape of the SEBS domains, the effect of C20A is evident by comparing Figure 1b and Figure 4b. In the binary blends the elastomer domains were nearly spherical. After adding C20A, they become ellipsoidal with an average aspect ratio of 0.55 ± 0.18. The average size can be computed as the elliptical area of the droplets as observed in the STXM images. In the case of the circular droplets in binary PP/SEBS blends, the average area was 0.6 ± 0.1 μm^2 for 90/10 and 0.8 ± 0.1 μm^2 for 80/20. In the case of the ternary PP/C20A/SEBS composites, the average area is 0.27 ± 0.06 μm^2.

From Figure 4b, it is clear that SEBS is wetting the clay stacks, surrounding them, and adopting their shape. We can also observe that in the presence of montmorillonite the SEBS domains are better dispersed. MMT produces a

reduction of SEBS domains size slowing down their tendency to coalescence. This is attributed to an increase in melt viscosity after adding MMT which affects the dispersion of the elastomer phase.[45−47]

Regarding the role of the polymers in the C20A intercalation, we now know that SEBS surrounds the nanoclay hindering the dispersion of C20A in the PP matrix. Therefore, only SEBS chains can intercalate the montmorillonite, which is contained in the SEBS droplets. The interpretation of the twisted structure observed in the TEM image of Figure 3d is now straightforward: inside the SEBS domains, the C20A layers tend to twist owing to the expansive action of SEBS that prevents the C20A layers from opening and dispersing in the PP matrix. Hence, we conclude that SEBS does not behave as a compatibilizer agent because, although the elastomer intercalates the C20A, SEBS encapsulates it and the clay is not in direct contact with the PP phase.

The reason for C20A to interact with SEBS rather than with PP might be the higher polarity and surface energy of styrene in comparison with the poliolefinic components (Table 1[40]). In blends like PA6/ABS,[48] PA6/PP,[49] and PP/funcionalizated EPR,[50] it has been observed that the montmorillonite locates selectively in the phase it has more affinity with. The key for a successful dispersion of nanoclay in a polymer matrix seems to be the presence of polar groups homogeneously distributed in the matrix, either because they are intrinsically in the matrix polymers (as is the case in polyamides) or because they are added in the form of a compatilizer agent miscible in the matrix, as is the case for PP grafted with maleic anhydride for a PP matrix.[1] In the case discussed here, styrene groups permit the SEBS to surround the C20A montmorillonite easily, but the interaction seems to be too strong and the processing conditions result insufficient to disperse the clay within the matrix. In recent work about thermoplastic matrixes and some type of montmorillonite, the use of SEBS grafted with maleic anhydride results in nanocomposites with intercalated[51,52] structure or partially exfoliated.[53]

Conclusions

An investigation of the structure and morphology of PP/C20A/SEBS nanocomposite prepared by melt processing has been carried out with special emphasis on the structure of the interface. STXM has been used to provide images and spatially resolved compositional information simultaneously of the three components and has allowed determining the role of SEBS in the nanocomposite structure.

From the XRD experiments, an intercalated structure was determined for the nanocomposite. TEM observations showed a mixed morphology in which stacks coexisted with intercalated regions and some individual exfoliated layers. However, the nanoclay was not well dispersed in the matrix, and it was not possible to distinguish which polymer was interacting with it. The stacks did not appear lined up but bent and twisted, and the clay exfoliation seemed to be hindered.

The NEXAFS microscopy experiments clearly showed that the elastomer is surrounding the nanoclay, and although inside the rubbery phase there is intercalation, SEBS does not act as a compatibilizer agent since C20A is not in contact with PP. The dispersion of the montmorillonite in the PP matrix is dominated by the compatibility between the polymeric components and the nanoclay. On the other hand, the presence of the nanoclay causes a decrease in the coalescence of the rubbery phase. There is a reduction of the size of SEBS domains in comparison with binary PP/SEBS systems, and these domains are better distributed in the PP matrix.

Acknowledgment. This work has been supported by the I3P-CSIC predoctoral program and has been partially financed by project FOREMOST (Contract NMP3-CT-2005-515840) from the EU FP6 programme and the Spanish MICINN for national project (MAT2006-13167-C01). We are indebted to J. González-Casablanca and R. Castro from Universidad Rey Juan Carlos (URJC) of Madrid for their assistance in the use of the TEM. We also acknowledge the assistance of Daniel Henández-Cruz, Sufal Swaraj, and Benjamin Watts at the BL-5.3.2 STXM of the ALS, which is supported by the Director of the Office of Science, Department of Energy, under Contract DE-AC02-05CH11231. Work at NCSU is supported by DOE, OS, BES, DMSE under Grant DE-FG0298ER45737.

References and Notes

(1) Martin, Z.; Jiménez, I.; Gómez, M. A.; Ade, H.; Kilcoyne, A. L. D.; Hernández-Cruz, D. *J. Phys. Chem. B* **2009**, *113*, 11160–11165.
(2) Vaia, R. A.; Jandt, K. D.; Kramer, E. J.; Giannelis, E. P. *Macromolecules* **1995**, *28*, 8080–8085.
(3) Ray, S. S.; Okamoto, M. *Prog. Polym. Sci.* **2003**, *28*, 1539–1641.
(4) Thostenson, E. T.; Chou, C. L. T.-W. *Compos. Sci. Technol.* **2005**, *65*, 491–516.
(5) Kalaitzidou, K.; Fukushima, H.; Miyagawa, H. *Polym. Eng. Sci.* **2007**, *47*, 1796–1803.
(6) Vaia, R. A.; Giannelis, E. P. *Macromolecules* **1997**, *30*, 8000–8009.
(7) Xu, W.; Guodong, L.; Wang, W.; Tang, S.; He, P.; Pan, W.-P. *J. Appl. Polym. Sci.* **2005**, *88*, 3225–3231.
(8) Modesti, M.; Lorenzetti, A.; Bon, D.; Besco, S. *Polymer* **2005**, *46*, 10237–10245.
(9) Park, J. U.; Choi, Y. S.; Cho, K. S.; Kim, D. H.; Ahn, K. H.; Lee, S. J. *Polymer* **2006**, *47*, 5145–5153.
(10) Rzaev, Z. M. O.; Yilmazbayhan, A.; Alper, E. *Adv. Polym. Sci.* **2007**, *26*, 41–55.
(11) Okada, A.; Fukushima, Y.; Kawasumi, M.; Inagaki, S.; Usuki, A.; Sugiyama, S.; Kurauchi, T.; Kamigaito, O. Patent US4739007, Toyota Motor Co., Japan, **1988**.
(12) Sung, Y. T.; Kim, Y. S.; Lee, K.; Dim, W. N.; Lee, H. S.; Sung, J. Y.; Yoon, H. G. *Polym. Eng. Sci.* **2007**, *47*, 1671–1677.
(13) Mittal, V. *J. Appl. Polym. Sci.* **2008**, *107*, 1350–1361.
(14) Hasegawa, N.; Kawasumi, M.; Kato, M.; Usuki, A.; Okada, A. *J. Appl. Polym. Sci.* **1998**, *67*, 87–92.
(15) Rapoport, L.; Nepomnyashchy, O.; Verdyan, A.; Popovitz-Biro, R.; Volovik, Y.; Ittah, B.; Tenne, R. *Adv. Eng. Mater.* **2004**, *6*, 44–48.
(16) Jang, B. N.; Wang, D.; Wilkie, C. A. *Macromolecules* **2005**, *38*, 6533–6543.
(17) Kim, D. H.; Fasulo, P. D.; Rodgers, W. R.; Paul, D. R. *Polymer* **2007**, *48*, 5308–5323.
(18) Dubnikova, I. L.; Berezina, S. M.; Korolev, Y. M.; Dim, G. M.; Lomakin, S. M. *J. Appl. Polym. Sci.* **2007**, *105*, 3834–3850.
(19) Treece, M. A.; Zhang, W.; Moffitt, R. D.; Oberhauser, J. P. *Polym. Eng. Sci.* **2007**, *47*, 898–911.
(20) Kawasumi, M.; Hasegawa, N.; Kato, M.; Usuki, A.; Okada, A. *Macromolecules* **1997**, *30*, 6333–6338.
(21) Nam, P. H.; Maiti, P.; Okamoto, M.; Kotaka, T.; Hasegawa, N.; Usuki, A. *Polymer* **2001**, *42*, 9633–9640.
(22) Lu, Q. W.; Macosko, C. W. *Polymer* **2004**, *45*, 1981–1991.
(23) Varela, C.; Rosales, C.; Perera, R.; Matos, M.; Poirier, T.; Blunda, J.; Rojas, H. *Polym. Compos.* **2006**, *27*, 451–460.
(24) Borggreve, R. J. M.; Gaymans, R. J.; Eichenwald, H. M. *Polymer* **1989**, *30*, 78–83.
(25) Liang, J. Z. *J. Appl. Polym. Sci.* **2000**, *77*, 409–417.
(26) Ray, S. S.; Pouliot, S.; Bousmina, M.; Utracki, L. A. *Polymer* **2004**, *45*, 8403–8413.
(27) Hong, S. H.; Namkung, H.; Ahn, K. H.; Lee, S. J.; Kim, C. *Polymer* **2006**, *47*, 3967–3975.
(28) Araki, T.; Ade, H.; Stubbs, J. M.; Sundberg, D. C.; Mitchell, G. E.; Kortright, J. B.; Kilcoyne, A. L. D. *Appl. Phys. Lett.* **2006**, *89*, 124106.
(29) Si, M.; Araki, T.; Ade, H.; Kilcoyne, A. L. D.; Fisher, R.; Sokolov, J. C.; Rafailovich, M. H. *Macromolecules* **2006**, *39*, 4793–4801.
(30) Ade, H.; Hitchcock, A. P. *Polymer* **2008**, *49*, 643–675.
(31) Ade, H.; Zhang, X.; Cameron, S.; Costello, C.; Kirz, J.; Williams, S. *Science* **1992**, *258*, 972–975.
(32) Kissinger, J. B.; Hughes, R. E. *J. Phys. Chem.* **2002**, *63*, 1959.

(33) Liang, Z. M.; Yin, J.; Xu, H. J. *Polymer* **2003**, *44*, 1391–1399.
(34) Rodriguez-Medellin, F. J.; Mata-Padilla, J. M.; Hsiao, B. S.; Waldo-Mendoza, M. A.; Vargas-Ramirez, E.; Baldes-Sanchez, S. *Polym. Eng. Sci.* **2007**, *47*, 1889–1897.
(35) Warwick, T.; Ade, H.; Kilcoyne, D.; Kritscher, M.; Tylisczcak, T.; Fakra, S.; Hitchcock, A.; Hitchcock, P.; Padmore, H. *J. Synchrotron Radiat.* **2002**, *9*, 254–257.
(36) Kilcoyne, A. L. D.; Tyliszczak, T.; Steele, W. F.; Fakra, S.; Hitchcock., P.; Franck, K.; Anderson, E.; Harteneck, B.; Rightor, E. G.; Mitchell, G. E.; Hitchcock, A. P.; Yang, L.; Warwick, T.; Ade, H. *J. Synchrotron Radiat.* **2003**, *10*, 125–136.
(37) Dhez, O.; Ade, H.; Urquhart, S. G. *J. Electron Spectrosc. Relat. Phenom.* **2003**, *128*, 85.
(38) Fanegas, N.; Gómez, M. A.; Jiménez, I.; Marco, C.; García-Martínez, J. M.; Ellis, G. *Polym. Eng. Sci.* **2008**, *48*, 80–87.
(39) Wu, D.; Zhou, C.; Zhang, M. J. *J. Appl. Polym. Sci.* **2006**, *102*, 3628–3633.
(40) Mark, J. E. *Polymer Data Handbook*, 2nd ed.; Oxford University Press: New York, 1999.
(41) Turner-Jones, A.; Aizlewood, J. M.; Beckett, D. R. *Macromol. Chem.* **1964**, *75*, 134–158.
(42) Avrami, M. *J. Chem. Phys.* **1940**, *8*, 212–224.
(43) Golebiewski, J.; Galeski, A. *Compos. Sci. Technol.* **2007**, *67*, 3442–3447.
(44) www.nanoclay.com.
(45) Sung, Y. T.; Kim, Y. S.; Lee, K.; Dim, W. N.; Lee, H. S.; Sung, J. Y.; Yoon, H. G. *Polym. Eng. Sci.* **2007**, *47*, 1671–167.
(46) Lee, H.-S.; Fasulo, P. D.; Rodgers, W. R.; Paul, D. R. *Polymer* **2005**, *46*, 11673–11689.
(47) Lee, H.-S.; Fasulo, P. D.; Rodgers, W. R.; Paul, D. R. *Polymer* **2006**, 3528–3539.
(48) Li, Y.; Shimizu, H. *Macromol. Rapid Commun.* **2005**, *26*, 710–715.
(49) Dharaiya, D.; Jana, S. C. *ANTEC* **2005**, *63*, 1439–1443.
(50) Kontopoulou, M.; Liu, Y.; Austin, J. R.; Parent, J. S. *Polymer* **2007**, *48*, 4520–4528.
(51) Tjong, S. C.; Bao, S. P. *Compos. Sci. Technol.* **2007**, *67*, 314–323.
(52) Farahani, R. D.; Ramazani, A. *Mater. Des.* **2008**, *29*, 105–111.
(53) Bao, S. P.; Tjong, S. C. *Composites, Part A* **2007**, *38*, 378–387.